

**Near-infrared light-triggered drug release nanogels for
combined photothermal-chemotherapy of cancer**

Journal:	<i>Biomaterials Science</i>
Manuscript ID:	BM-ART-02-2015-000048.R1
Article Type:	Paper
Date Submitted by the Author:	17-Mar-2015
Complete List of Authors:	Zan, Minghui; Anhui Normal University, College of Chemistry and Materials Science; Anhui Normal University, College of Chemistry and Materials Science Li, Junjie; University of Science and Technology of China, Department of Polymer Science and Engineering Huang, Mingming; University of Science and Technology of China, Department of Polymer Science and Engineering Lin, Shanqing; University of Science and Technology of China, Department of Polymer Science and Engineering Luo, Dan; Hospital of Anhui Province, Department of Ophthalmology luo, shizhong; Anhui Normal University, College of Chemistry and Materials Science Ge, Zhishen; University of Science and Technology of China, Department of Polymer Science and Engineering

Cite this: DOI: 10.1039/c0xx00000x

www.rsc.org/xxxxxx

ARTICLE TYPE

Near-infrared light-triggered drug release nanogels for combined photothermal-chemotherapy of cancer

Minghui Zan,^{a,b} Junjie Li,^b Mingming Huang,^b Shanqing Lin,^b Dan Luo,^{*c} Shizhong Luo^{*a} and Zhishen Ge^{*b}

⁵ Received (in XXX, XXX) Xth XXXXXXXXX 20XX, Accepted Xth XXXXXXXXX 20XX

DOI: 10.1039/b000000x

Near-infrared (NIR) light-triggered drug release systems are promising for drug delivery applications in view of advantages of NIR light with high tissue penetration and low damage. In this report, we developed nanogels (NGs) by supramolecular self-assembly from adamantane (AD)-conjugated copolymer, poly[poly(ethylene glycol)monomethyl ether methacrylate]-*co*-poly(*N*-(2-hydroxypropyl)methacrylamide)-*co*-poly(*N*-adamantan-1-yl-2-methacrylamide) (PPEGMA-*co*-PHPMA-*co*-PADMA), and β -cyclodextrin (β -CD)-functionalized poly(amidoamine) (PAMAM) dendrimer based on host-guest interaction of AD and β -CD moieties, which were used to encapsulate indocyanine green (ICG) and doxorubicin (DOX) for combined photothermal-chemotherapy. NGs simultaneously loading ICG and DOX (DINGs) showed significant photothermal effect and stimuli-triggered drug release under NIR laser irradiation by photothermal-induced relaxation or dissociation of NGs. *In vitro* cytotoxicity evaluation of DINGs under NIR irradiation demonstrated synergistic effect of hyperthermia, photothermal-triggered drug release, and chemotherapy. *In vivo* investigation revealed their high accumulation in tumor tissue and significant tumor growth suppression under NIR irradiation. The NIR light-triggered drug release NGs represent efficient and promising anticancer drug vectors for combined photothermal-chemotherapy of cancer to maximize therapeutic efficacy and minimize side effects.

Introduction

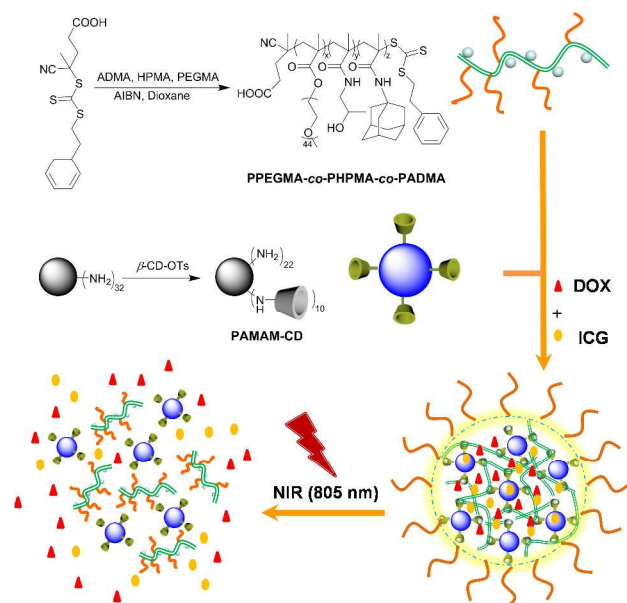
Finely engineered polymeric nanocarriers as anticancer drug delivery system frequently offer clinically used anticancer drugs distinct properties mainly including enhanced water solubility as well as optimized organ distribution and pharmacokinetics.¹⁻⁴ However, conventional nanocarriers tend to release encapsulated drugs passively, which could not be controlled for best therapeutic efficacy. Stimuli-responsive nanocarriers could achieve controllable drug release through endogenous or exogenous stimuli.⁵⁻⁸ The adverse side effects can be minimized simultaneously maximizing their therapeutic efficacy via on-demand drug release. Among various stimuli, light-responsive nanocarriers attracted much interest due to highly temporal and spatial control over drug release. Light-triggered release from nanocarriers was achieved frequently by the strategy of light-responsive structural transformation, resulting in properties variation such as hydrophilic/hydrophobicity reversal or cleavage of chemical bonds.^{9,10} To this end, short-wavelength lights such as UV or visible light were usually used because high-frequency light for sufficient energy was needed. However, the application of UV or visible light was limited due to poor tissue penetration. To overcome these limitations, near-infrared (NIR) light in the wavelength range of 750-1300 nm is particularly attractive due to deep tissue penetration. However, for improving light energy, the

transformation of NIR light by simultaneous two-photo absorbance or introduction of upconverting nanoparticles had to be performed.¹¹⁻¹³ Notably, the effective two-photo absorbance required high-power lasers and inconvenient operation. The utility of upconverting nanoparticles has to incorporate highly toxic rare-earth elements into delivery systems. Therefore, the disadvantages limited wide use of these strategies.

On the other hand, another strategy is to utilize photothermal effects of nanocarriers under NIR irradiation as a trigger for thermo-responsive release.¹⁴⁻²¹ Gold or other inorganic nanoparticles were frequently used to absorb NIR light for efficient heat generation,¹⁴⁻¹⁹ which possessed some intrinsic concerns of metal nanoparticles. Recently, NIR light-absorbed biocompatible organic small molecules were introduced into polymeric nanoparticle for NIR-light absorption and heat generation. For example, indocyanine green (ICG) as a widely used water-soluble dye approved by the United States Food and Drug Administration has been recently explored for NIR-light absorption and photothermal therapy of cancers.²²⁻²⁴ Simultaneously, incorporation of ICG and anticancer drug into one nanocarriers could also achieve synergized photothermal-chemotherapy of cancer.²⁴⁻²⁶ Moreover, the encapsulated ICG in theranostic nanoparticle delivery systems can serve as fluorescent imaging agents to detect and track the biodistribution of nanoparticles.²³⁻²⁸ However, NIR light-triggered drug release systems based on ICG-loaded polymeric nanocarriers were rarely

exploited.

Supramolecular self-assembly based on host-guest interactions has been used to construct a diverse range of nanoparticles for drug delivery applications.²⁹⁻³² As compared with covalently cross-linked nanoparticles, preparation of supramolecular assemblies was demonstrated to be convenient and flexible. Among them, the molecular recognition between β -cyclodextrin (β -CD) and adamantane (AD) showed relatively strong interactions, high biocompatibility, and reversible dissociation.^{29,30,33,34} The supramolecular nanoparticles on the basis of interaction between β -CD and AD have been explored to encapsulate a variety of diagnostic or therapeutic agents.^{35,36} Tseng et al. further demonstrated disassembly of the nanoparticles by magnetothermal stimuli for on-demand drug release because high temperature led to weakened interaction between β -CD and AD.³⁵



Scheme 1 Schematic illustration of the nanogel fabrication from PPEGMA-co-PHPMA-co-PADMA copolymers and PAMAM-CD dendrimers, which were used to simultaneously encapsulate DOX and ICG showing NIR light-triggered drug release due to photothermal-induced relaxation of β -CD and AD-based host-guest interactions.

Herein, we constructed host-guest interaction-associated nanogels from AD-conjugated random copolymers, poly[poly(ethylene glycol)monomethyl ether methacrylate]-co-poly(*N*-(2-hydroxypropyl)methacrylamide)-co-poly(*N*-adamantan-1-yl-2-methacrylamide) (PPEGMA-co-PHPMA-co-PADMA), and β -CD-functionalized poly(amidoamine) dendrimer (PAMAM-CD), which were used to simultaneously encapsulate ICG and DOX (Scheme 1). ICG and DOX can be encapsulated into NGs (DINGs) with high encapsulation efficiencies (EEs) due to electrostatic interactions between PAMAM, DOX, and ICG.³⁷ Upon NIR irradiation at the wavelength of 805 nm, solution temperature increased significantly due to NIR light absorption and transformation into heat. At elevated temperatures, dissociation of the nanogels occurred due to weakened interaction between β -CD and AD moieties.^{38,39} The encapsulated DOX can be released in a controllable fashion. Thus, synergized photothermal therapy and chemotherapy can be expected with

NIR light-triggered drug release. *In vitro* cytotoxicity evaluation exhibited synergistic effect of photothermal therapy, photothermal-triggered drug release, and chemotherapy. Confocal laser scanning microscopy (CLSM) observation showed that DOX localized in the cell nucleus quickly after cellular uptake of DINGs and NIR irradiation. *In vivo* cancer treatment evaluation of DINGs showed high accumulation in tumor tissue and significant tumor growth suppression under periodic NIR irradiation.

Experimental section

Materials

Triethylamine (TEA), tetrahydrofuran (THF), 1,4-dioxane, dichloromethane (DCM), methanol, and dimethyl sulfoxide (DMSO) were dried and distilled prior to use. 2,2'-Azobisisobutyronitrile (AIBN, 98%, Fluka) was recrystallized from 95% ethanol. β -Cyclodextrin (β -CD) was recrystallized from distilled water. 1-Adamantylamine hydrochloride (98%) was purchased from Aladdin Reagent Company and used as received. Methacryloyl chloride was purchased from Aladdin Reagent Company and distilled prior to use. Third generation poly(amidoamine) dendrimer (G3 PAMAM), indocyanine green (ICG), and doxorubicin hydrochloride (DOX) was purchased from Sigma-Aldrich and used as received. Poly(ethylene glycol) monomethyl ether methacrylate (PEGMA) (average $M_n \sim 2,000$),⁴⁰ *N*-(2-hydroxypropyl) methacrylamide (HPMA),⁴¹ 4-cyano-4-(2-phenylethane sulfanylthiocarbonyl) sulfanyl pentanoic acid (PETTC),⁴² *N*-(1-Adamantyl) methacrylamide (ADMA),⁴³ and monotosylated β -CD (β -CD-OTs)⁴⁴ were synthesized according to established procedures provided in the literatures. Fetal bovine serum (FBS), trypsin, phosphate buffered saline (PBS), and Dulbecco's modified Eagle's medium (DMEM) were purchased from GIBCO and used as received. Cell culture lysis buffer, 4',4',6-diamidino-2-phenylindole (DAPI), 3-(4,5-dimethylthiazol-2,5-diphenyltetrazolium bromide (MTT), propidium iodide (PI, 94%), fluorescein diacetate (FDA), and Hematoxylin and Eosin (H&E) Staining Kit were purchased from Beyotime Institute of Biotechnology (Shanghai, China). All other commercially available solvents and reagents were purchased from Sinopharm Chemical Reagent Co. Ltd. and used as received. The murine hepatic cancer cell line, H22, and HepG2 cells were purchased from Shanghai Institute of Cell Biology (Shanghai, China). Male 6-week-old CD-1 (ICR) mice were purchased from Vital River Laboratory Animal Technology Co. Ltd. (Beijing, China). The animal studies were carried out in accordance with the Regulations for the Administration of Affairs Concerning Experimental Animals (Hefei, revised in June 2013) and adhered to the Guiding Principles in the Care and Use of Animals of the American Physiological Society.

Synthesis of PPEGMA-co-PHPMA-co-PADMA

The synthetic routes employed for the preparation of PPEGMA-co-PHPMA-co-PADMA random copolymer were shown in Scheme 1. Briefly, PPEGMA-co-PHPMA-co-PADMA random copolymer was prepared by reversible addition-fragment chain transfer (RAFT) polymerization of PEGMA, HPMA and ADMA using PETTC as the chain transfer agent (CTA). To a Schlenk tube equipped with a magnetic stirring bar, PEGMA (3.12 g, 1.5

mmol), HPMA (2.15 g, 15 mmol), ADMA (0.66 g, 3 mmol), PETTC (33.9 mg, 0.1 mmol), and AIBN (2.6 mg, 0.016mmol) was dissolved in the mixture of 1,4-dioxane and methanol (5 mL, 4/1, v/v). The reaction tube was carefully degassed by three freeze-pump-thaw cycles, sealed under vacuum, and placed in an oil bath thermostated at 80 °C. After stirring for 20 h, the ampoule was quenched into liquid nitrogen to terminate the polymerization. The mixture was precipitated into an excess of ether. The above dissolution-precipitation cycle was repeated for three times. The obtained solids were further purified by dialysis against distilled water for three days using a dialysis bag (MWCO: 10 kDa). The solution was lyophilized, affording PPEGMA-co-PPHMA-co-PADMA as a white powder (3.6 g, yield: 61.0%; $M_{n,GPC} = 41.6$ kDa, $M_w/M_n = 1.14$). The actual degrees of polymerization (DPs) of PPEGMA, PPHMA and PADMA segments were determined to be 12, 94, and 21, respectively, by ^1H NMR analysis in D_2O . Thus, the polymer was denoted as PPEGMA₁₂-co-PPHMA₉₄-co-PADMA₂₁.

Synthesis of PAMAM-CD

The G3 PMAMA dendrimer was reacted with β -CD-OTs according to the previous reports.^{45,46} Briefly, G3 PAMAM dendrimer (200 mg, 2.89×10^{-5} mol) in methanol and β -CD-OTs (1.79 g, 1.39 mmol) were dissolved in distilled DMSO (10 mL). The mixture was stirred for 4 days at 60 °C under the protection of N_2 atmosphere. The β -CD-conjugated PAMAM dendrimer was purified by Sephadex G-75 column with 0.1 M Na_2SO_4 aqueous solution as the eluent followed by 3 days dialysis in distilled water using a dialysis bag (MWCO: 10 kDa). After lyophilization, the final product was obtained as a pale yellow solid (0.56 g, yield: 28%). The number of β -CD moieties in a PAMAM-CD molecule was determined to be 10 on the basis of ^1H NMR analysis in D_2O .

Preparation of supramolecular NGs and drug encapsulation

DMSO solution (1 mL) containing PAMAM-CD (4.6 mg), DOX (3 mg), and ICG (3 mg) was added dropwise into PBS (9 mL, pH 7.4) containing PPEGMA-co-PPHMA-co-PADMA (5 mg) at β -CD/AD molar ratio of 1:1 under vigorous stirring. The mixture was kept at 70 °C for 30 min, followed by annealing at room temperature for 3 h. Subsequently, the obtained mixture was dialyzed against distilled water for 2 h using a dialysis bag (MWCO: 6000 Da). Finally, NGs were purified to remove nonencapsulated molecules using centrifugation separation via ultrafiltration membrane (Cut-off 100 K MW) at 3000 rpm. The NGs encapsulated both ICG and DOX were denoted as DINGs. Moreover, NGs only encapsulated ICG or DOX were also prepared according to similar procedures, which were denoted as INGs and DNGs, respectively. Free DOX/ICG was obtained by simply mixing DOX and ICG in PBS.

The encapsulation efficiencies (EEs) and loading efficiencies (LEs) of DOX or ICG loaded in NGs were determined. Briefly, after recovering the filtrate without nonencapsulated DOX and ICG, the encapsulated amounts of DOX and ICG were analyzed after dissolving in DMSO by absorbance at a wavelength of 480 nm and 780 nm, respectively. EEs and LEs were calculated according to the following formula: $\text{EE} (\%) = ((\text{weight of loaded drug})/(\text{weight of initially added drug})) \times 100\%$; $\text{LE} (\%) = ((\text{weight of loaded drug})/(\text{total weight of DINPs})) \times 100\%$.

Characterization

All nuclear magnetic resonance (NMR) spectra were recorded on a Bruker AV300 NMR 300 MHz spectrometer using D_2O , $\text{DMSO}-d_6$, or CDCl_3 as the solvent. The molecular weights (MWs) and molecular weight distributions (M_w/M_n) of PPEGMA-co-PPHMA-co-PADMA were determined by gel permeation chromatography (GPC) equipped with an Agilent1260 pump and an Agilent G1362A differential refractive index detector. The eluent was DMF with 1 g/L LiBr at a flow rate of 1.0 mL/min. A series of low polydispersity PEG standards were employed for calibration. The particles size of the nanogels was measured by the dynamic light scattering technique (DLS) using a Zetasizer Nano ZS instrument, equipped with a He-Ne ion laser ($\lambda = 632$ nm) at a scattering angle of 173°. Transmission electron microscopy (TEM) observation was conducted using a Hitachi H-800 electron microscope at an acceleration voltage of 200 kV for insight on the morphology of the particles. The copper TEM grids were dipped into desired samples. The sample grids were blotted by filter paper to remove excess complex solution, followed by drying for 1 hour. As for observation of DINGs after irradiation, a droplet of solution was dripped on the copper grid, followed by irradiation under NIR laser light of 805 nm for 3 min until the solutions were dried sufficiently. The laser with the center wavelength of 805 nm and fibers were purchased from Changchun Laser Optoelectronics Technology Co., Ltd (Changchun, China). The laser power density was mainly controlled by the output power and affected by the beam spot size. A laser energy/power meter (PhyScience Opto-Electronics, Beijing, China) was used to measure the power density which was fixed at 1.5 W/cm^2 by controlling the output power and beam spot size.

Photothermal effect

DINPs, INPs, and free DOX/ICG at the various ICG concentrations (5, 10, and 20 $\mu\text{g}/\text{mL}$) were stored in the transparent plastic vials and then were irradiated at the wavelength of 805 nm ($1.5 \text{ W}/\text{cm}^2$). Simultaneously, temperature of the solution was monitored using YCT data logger thermometer within 300 s. PBS was used as the negative control.

In vitro drug release profiles

In vitro release of DOX from DINPs under different conditions was studied using a dialysis bag diffusion method. In brief, DINPs solution (0.5 mL) containing 0.22 mg DOX and 0.2 mg ICG was injected into a pre-swelled dialysis bag with a molecular weight cutoff of 6 kDa, followed by immersion into 19.5 mL of 10 mM PBS (pH 7.4). The dialysis was conducted at 37 °C in a shaking culture incubator. NIR laser irradiation was applied to the sample for 3 min at predetermined time points (0, 4, 8, and 12 h). DINPs without laser irradiation were used as control. Periodically, 1 mL aliquot of sample solution from the incubation medium was taken for measurements and compensated with 1 mL of fresh buffer to incubation medium every 2 h. The amount of released DOX was determined by fluorescence intensity. The DOX release from DINPs was expressed as the percentage of cumulative DOX outside the dialysis bag to the total DOX in the DINPs solutions.

In vitro cytotoxicity evaluation

HepG2 cells were seeded onto 96-well plates at a density of 1×10^4 cells/well in 100 μ L DMEM with 10% FBS at 37 $^{\circ}$ C with 5% CO₂ humidified atmosphere. After 24 h incubation, the original medium was replaced with fresh culture medium. Then, the 5 different formulations including polymers (PPEGMA-*co*-PHPMA-*co*-PADMA and PAMAM-CD), free DOX/ICG, INGs, DNGs, and DINGs at various concentrations were added into each well in a concentration-dependent manner. After 12 h incubation, the medium was removed, followed by addition of 10 fresh medium. As for laser irradiation groups, the cells were exposed to 1.5 W/cm² laser and irradiated for 3 min, followed by incubation for another 24 h. For fluorescence microscopy investigation, the medium was replaced with 100 μ L PBS. Then, each well was treated with 1 μ L FDA solution (1 mg/mL in 15 DMSO) and continued to be incubated for 20 min at 37 $^{\circ}$ C in the dark. Subsequently, PBS was removed and 2 μ L of propidium iodide (PI) solution (1 mg/mL in DMSO) was added to each well followed by 10 min incubation. Finally, each well was washed with PBS twice and then observed by fluorescence microscopy 20 (Olympus inverted microscope IX-71).

For MTT assay, MTT solution (20 μ L, 5 mg/mL in PBS buffer) was added to each well and incubated 4 h for reaction. The medium in each well was then removed and 200 μ L of DMSO was added to dissolve the internalized purple formazan 25 crystals. The plate was subjected to gently agitation for 30 min until all the crystals were dissolved. The absorbance at wavelength of 480 nm was recorded by a microplate reader (Thermo Fisher).

Cellular internalization and intracellular distribution of the 30 micelles using CLSM

Cellular internalization and intracellular distribution of the micelles in HepG2 cells were observed using CLSM. HepG2 cells were seeded at a density of 1×10^4 cells/well into a 35-mm glass-bottom culture dish and cultured overnight in 2 mL DMEM 35 medium with 10% FBS at 37 $^{\circ}$ C with 5% CO₂ humidified atmosphere. Then, the medium was replaced by the fresh culture medium, followed by addition of free DOX (8.6 μ g/mL), free ICG (8 μ g/mL), or DINPs (8.6 μ g/mL of DOX and 8 μ g/mL of ICG), respectively. After 4 h internalization, the cells were 40 washed with ice-cold PBS. Half of the cells treated with DINPs was exposed to an 805 nm laser irradiation at a power density of 1.5 W/cm² for 3 min, followed by adding the fresh culture medium and incubation for another 2 h. Then the cells fixed with 4% paraformaldehyde solution for 20 min, washed for three times 45 with ice-cold PBS. The cell nuclei was counterstained with DAPI (blue). Finally, cells were washed three times with ice-cold PBS and observed by CLSM (Zeiss LSM710).

Tumor Models

Male 6-week-old CD-1 (ICR) mice were inoculated 50 subcutaneously with 4×10^6 H22 cells suspended in 200 μ L PBS at the right flank to prepare the tumor models. The tumor volume (V) was calculated as follows: $V = a \times b^2 / 2$, where a is the tumor dimension at the longest point, and b is the tumor measurement at the widest point, as measured by a digital vernier caliper.

In vivo imaging

The mice were randomly divided into four groups. Mice in group

1 as control was intravenously injected with 200 μ L of PBS. Mice in group 2, group 3 and group 4 were intravenously injected with 200 μ L of free ICG, INGs and DINGs (both containing 1 mg/mL 60 ICG). The mice after injection at 24 h were sacrificed and the organs including heart, liver, spleen, lung, kidneys and tumor were collected for imaging analysis using Xenogen IVIS Lumina system (Caliper Life Sciences, Alameda, CA) with the excitation wavelength of 710 nm.

Antitumor effect by combined photothermal and 65 chemotherapy

When the tumors reached a size of 100 mm³ (about 8 days after transplantation), the mice were divided into five groups (four per group) that were intravenously injected with 200 μ L of PBS, 70 DINGs (containing 1 mg/mL ICG and 1.08 mg/mL DOX), INGs (containing 1 mg/mL ICG), free DOX (containing 1.08 mg/mL DOX) on day 0, 2, and 4, respectively. Subsequently, the tumors were irradiated or not by an 805-nm laser at the power density of 1.5 W/cm² for 5 min at 24 h post-injection. The tumor volumes of 75 each mouse were recorded. At day 16, mice were sacrificed and tumors were excised followed by sectioning into 10 μ m thick slices for H&E staining according to standard protocol and observed under fluorescent microscope.

Results and discussion

Polymer synthesis and self-assembly for preparation of drug- 80 loaded NGs

PPEGMA-*co*-PHPMA-*co*-PADMA random copolymer and PAMAM-CD dendrimer were designed for the preparation of NGs, where PHPMA and PPEGMA component served as the 85 water-soluble backbone to stabilize the self-assembled NGs, host-guest interactions between multiple AD and β -CD molecules were used to cross-link and form NGs. PPEGMA-*co*-PHPMA-*co*-PADMA was synthesized via RAFT polymerization and DP of each segment was determined from ¹H NMR spectra through 90 comparing the peak of benzene group (a) and peak d, b, f, respectively (Fig. 1A). The polymer was finally denoted as PPEGMA₁₂-*co*-PHPMA₉₄-*co*-PADMA₂₁. On the other hand, β -CD-OTs was conjugated onto the dendrimer, G3 PAMAM. The excess β -CD-OTs was removed by Sephadex G-75 column 95 followed by dialysis in water as evidenced by ¹H NMR. The number of conjugated β -CD on each PAMAM dendrimers was determined to be 10 according to ¹H NMR analysis Fig. 1B.

The self-assembly of PPEGMA-*co*-PHPMA-*co*-PADMA copolymer and PAMAM-CD for fabrication of nanogels were 100 carried out at an AD/ β -CD ratio of 1. It should be noted that if higher or lower AD/ β -CD ratios were used, the nanogels with bigger size and size distribution were obtained. Thus, in this work, we mainly prepared the nanogels at an AD/ β -CD ratio of 1. Simultaneously, drugs (ICG and DOX) encapsulation were 105 performed during self-assembly. When DOX was encapsulated, very low EE and LE were observed, which were 34.2% and 6.6%, respectively (Table 1). However, for ICG, high EE of 71.6% and LE of 13.8% were obtained due to the electrostatic interactions between negative ICG and positive PAMAM molecules.³⁷ 110 Interestingly, when DOX and ICG were simultaneously encapsulated into NGs, the EEs and LEs of DOX and ICG were both improved dramatically. Especially for DOX, upto 80.9% of

EE and 15.5% of LE were obtained. Presumably, DOX with positive charges can be encapsulated with dramatically improved efficiency presumably due to electrostatic interactions between ICG, DOX, and PAMAM.

DLS was used to characterize nanoparticles after self-assembly via host-guest interaction between AD and β -CD. After drug encapsulation of ICG and DOX, the average size of NGs was increased from 86.2 nm to 109.3 nm (Fig. 2). The morphologies of DINGs by TEM exhibited spherical shape with the average diameter of 63 nm which is smaller than that obtained from DLS due to the size shrinkage during drying process of sample preparation.

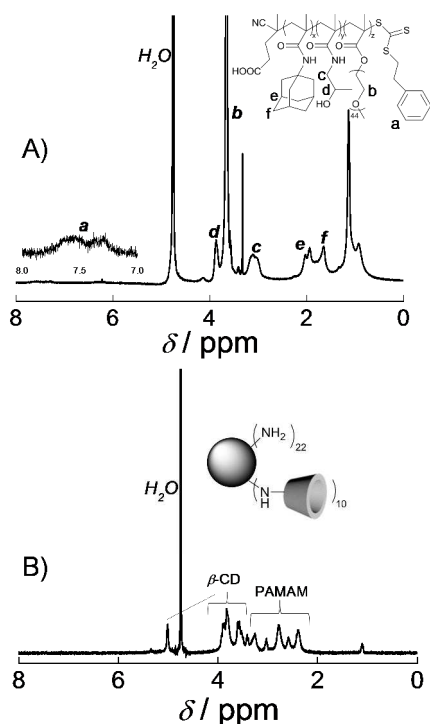


Fig. 1 ^1H NMR spectra recorded for (A) PHEMA-co-PADMA-co-PPEGMA copolymer and (B) PAMAM-CD dendrimer in D_2O .

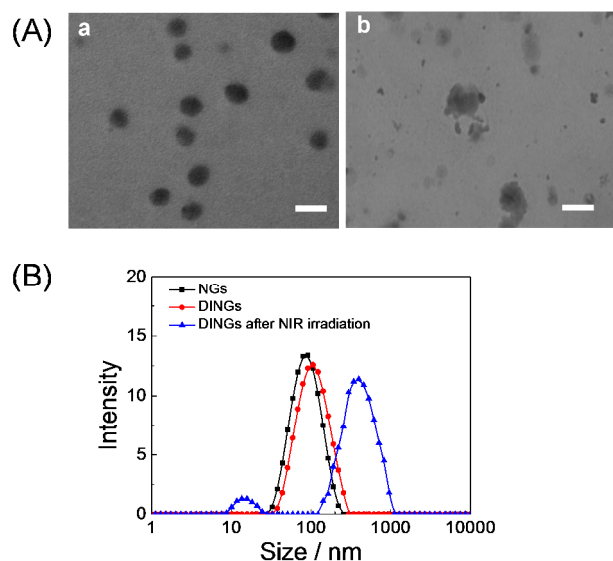


Fig. 2 (A) TEM images of DOX and ICG-encapsulated NGs (DINGs) before (a) and after (b) 805 nm NIR irradiation for 3 min. The scale bars

represent 100 nm. (B) Particle size distributions of NGs, DINGs, and DINGs after 805 nm NIR irradiation for 3 min.

NIR light-triggered NGs dissociation and drug release

ICG as a cyanine dye shows pronounced photothermal effect by the light irradiation in the NIR range.^{22,23} Free ICG showed a maximum absorbance peak at 780 nm (Fig. S1). After encapsulation into DINGs, the absorbance curve of ICG exhibited a red shift with the peak located at 795 nm, which is likely attributed to ICG aggregation between ICG and the polymers in the core of nanogels.^{47,48} Then, we evaluated the photothermal effect and temperature increment of PBS, free DOX/ICG, INGs, and DINGs at varying concentrations of ICG under 805 nm laser irradiation at a power density of 1.5 W/cm^2 (Fig. 3A). Within 300 s, the temperatures of PBS increased slightly. However, the formulations with ICG showed evident temperature increase upon irradiation. DINGs showed faster temperature increase than free ICG, presumably because the maximum absorption peak of free ICG at 780 nm shifted to 795 nm when encapsulated in nanogels, which is more close to the NIR wavelength used in this study (805 nm). The cooling effect after 4 min irradiation should be attributed to photodegradation and thermal degradation of ICG.^{48,49} On the other hand, it should be noted that the temperatures of DINGs cores where ICG molecules concentrated likely increased more rapidly after NIR irradiation as compared with the solution temperatures, which is favorable for nanogel dissociation.

Table 1 Characterization of DNGs, INGs, and DINGs.

NGs	Diameter/ nm	PDI	EE ^a of DOX/%	EE ^a of ICG/%	LE ^b of DOX/%	LE ^b of ICG/%
INGs	108.1	0.20	-	71.6	-	13.8
DNGs	121.4	0.16	34.2	-	6.6	-
DINGs	109.3	0.18	80.9	75.1	15.5	14.4

^a Encapsulation efficiency; ^b Loading efficiency.

We further investigated the morphology variation of NGs under NIR irradiation. TEM and DLS characterization indicated apparent dissociation of DINGs after 3 min NIR irradiation. Nanoparticles with nonuniform sizes from TEM images can be observed obviously (Fig. 2Ab). The DLS results showed broad size distribution with peaks located at smaller and bigger sizes (~ 10 nm and ~ 500 nm) (Fig. 2B). Presumably, the temperature increase under NIR irradiation resulted in weakened interaction between AD and β -CD, which finally led to relaxation or dissociation of DINGs.^{35,36} Therefore, on-demand drug release can be controlled by NIR light due to dissociation of DINGs activated by the local temperature increase. As shown in Fig. 3B, without NIR irradiation, slow drug release rate was observed with approximately 20% release after incubation for 16 h at 37 $^\circ\text{C}$. Then, we investigated the drug release profiles of DINGs under periodic NIR laser irradiation of 805 nm. After the first irradiation followed by 2 h incubation, 37.7% DOX release can be measured. Notably, after another 2 h incubation, drug release amount was only increased to 43.1% indicative of slow release rate without NIR irradiation. The controllable drug release in a stepwise fashion can be achieved by the NIR laser light irradiation. Considering high glass transition temperature of PHEMA, the NIR light-triggered release profiles of DOX from DINGs should be attributed to the reversible dissociation of

DINGs cross-linked by host-guest interactions between AD and β -CD moieties.^{35,50} Notably, even though ICG will generate reactive oxygen species (ROS) under NIR irradiation,⁴⁹ negligible influence on DOX activity was observed before and after NIR irradiation as evidenced by similar UV-vis absorbance curves (Fig S2).

Cytotoxicity of combined photothermal-chemotherapy

To evaluate the synergistic cytotoxicity of photothermal hyperthermia and chemotherapy against cancer cells, we measured the *in vitro* cytotoxicity of DINGs with or without NIR irradiation. First of all, the NIR power density of 1.5 W/cm² was demonstrated to show negligible influence on cell viability. The cells were then directly observed under fluorescence microscope after treatment of NGs by staining with FDA and PI for live cells (green) and dead/late apoptosis cells (red), respectively. As shown in Fig. 4A, the growth of cells in DNGs group was not affected evidently with and without NIR irradiation. In contrast, in DINGs group, a small population of cells were red without NIR irradiation possibly due to slow DOX release rate and low cytotoxicity against cancer cells. On the other hand, under NIR irradiation, the red regions in the picture were enlarged significantly as compared with no NIR irradiation. However, for free DOX/ICG group where both free ICG and DOX were used, NIR irradiation apparently had relatively smaller effect on cell viability.

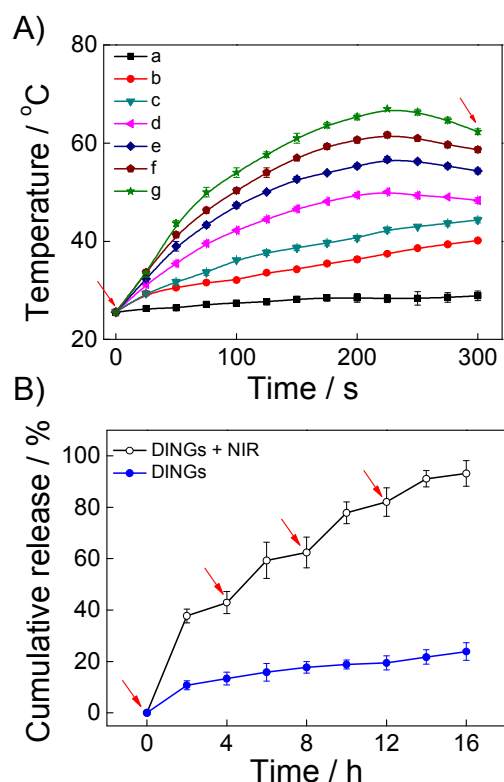


Fig. 3 (A) Temperature rise profiles of (a) PBS; (b) 5 μ g/mL of free DOX/ICG; (c) 5 μ g/mL of DINGs; (d) 10 μ g/mL of free DOX/ICG; (e) 10 μ g/mL of DINGs; (f) 20 μ g/mL of free DOX/ICG; (g) 20 μ g/mL of DINGs under NIR laser irradiation. The arrows indicated that the irradiation started or ended. (B) *In vitro* DOX release profiles from DINGs at pH 7.4 with periodic NIR laser irradiation. The curve without NIR irradiation was used as the control. The arrows indicated that 3 min

NIR laser irradiation was carried out. Data are expressed as mean \pm SD, n = 3.

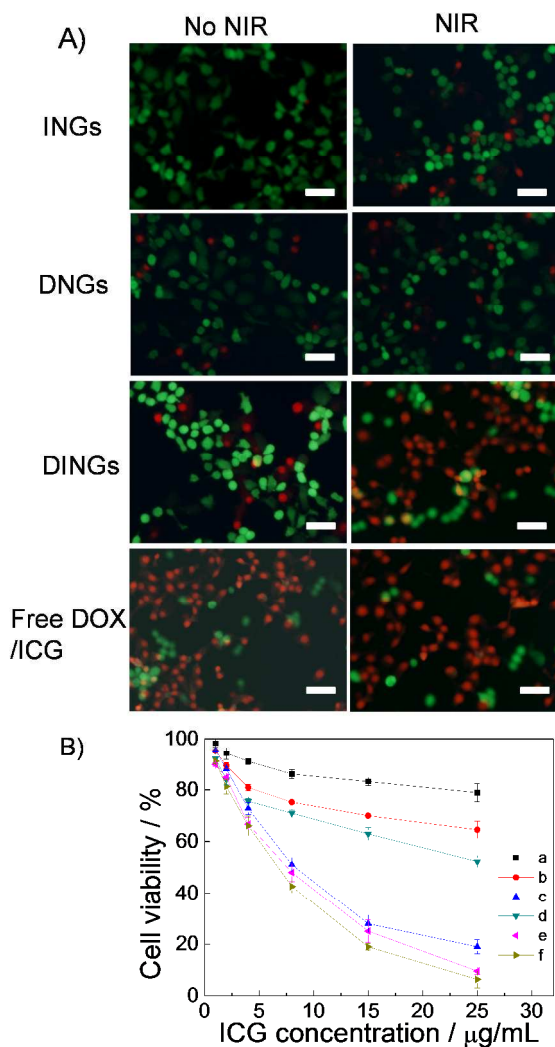


Fig. 4 HepG2 cancer cell survivals of the various treatment groups. (A) Fluorescence microscopy images of HepG2 cells after treatment using free DNGs (8.6 μ g/mL DOX), INGs (8 μ g/mL ICG), DINGs (8.6 μ g/mL of DOX and 8 μ g/mL of ICG), and free DOX/ICG (8.6 μ g/mL of DOX and 8 μ g/mL of ICG), respectively, with or without NIR irradiation for 3 min. Live cells were stained green with FDA, and dead/late apoptosis cells were stained red with PI. Scale bars represent 100 μ m. (B) Cell viability of HepG2 after treatment with (a) INGs; (b) DINGs (DOX/ICG = 4.3/4 w/w); (c) Free DOX/ICG (DOX/ICG = 4.3/4 w/w); (d) INGs with NIR irradiation; (e) DINGs with NIR irradiation (DOX/ICG = 4.3/4 w/w); (f) Free DOX/ICG with NIR irradiation (DOX/ICG = 4.3/4 w/w). Data are expressed as mean \pm SD, n = 4.

Cytotoxicity of all the formulations was further evaluated by MTT assay (Fig. 4B). INGs without NIR irradiation showed low cytotoxicity at various ICG concentrations indicating low toxicity of NGs and encapsulated ICG molecules. Under NIR irradiation, INGs exhibited less than 80% cell viability with ICG concentrations higher than 5 μ g/mL, which should be attributed to photothermal hyperthermia. Moreover, free ICG/DOX group showed high toxicity to cells without NIR irradiation and stronger cytotoxicity was observed after NIR irradiation. The IC₅₀ values of DOX concentration dropped from 7.7 μ g/mL to 5.8 μ g/mL after NIR irradiation. However, for DINGs, IC₅₀ of DOX was

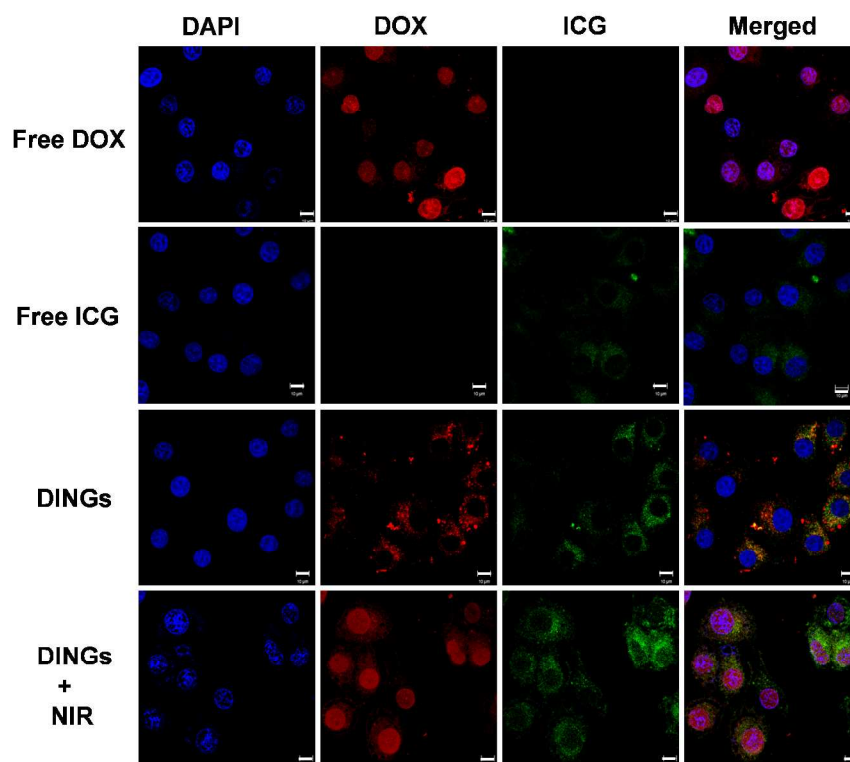


Fig. 5 CLSM observation of the intracellular distribution of free DOX, free ICG, DINGs, and DINGs with 805 nm NIR laser irradiation for 3 min in HepG2 cells. Nuclei (blue) were stained with DAPI.

5 decreased dramatically from 33 $\mu\text{g}/\text{mL}$ to 7 $\mu\text{g}/\text{mL}$ after application of NIR irradiation. The significantly higher influence of NIR irradiation on cytotoxicity of DINGs should be attributed to synergistic effect of combined photothermal-chemotherapy and NIR light-triggered drug release.

10 We further investigated DOX distribution in cells after internalization of DINGs followed by NIR irradiation by using CLSM. Red and green colors were used to distinguish DOX and ICG, respectively. As shown in Fig. 5, free ICG and DOX were internalized into the cells after 4 h incubation. Notably, a great deal of free DOX localized in cell nucleus due to high affinity
15 between DOX and DNA. For DINGs, nearly all internalized DOX was localized in cytoplasm after 4 h incubation without NIR irradiation while DOX could not be observed in nucleus. However, after NIR irradiation for 3 min followed by another 2 h
20 incubation, a great deal of DOX were observed to be localized in cell nucleus. These results suggested that NIR light-triggered DOX release of DINGs could be controlled by NIR irradiation in cells after internalization.

Antitumor efficacy by combined photothermal-chemotherapy

25 The biodistribution and tumor accumulation of NGs were firstly investigated after intravenous injection. DINGs were intravenously injected into the tumor-bearing mice, and the tumor was excised after 24 h followed by observation of ICG using IVIS imaging systems. Nearly all free ICG molecules were cleared from the body (Fig. S3). For INGs and DINGs, distinctly high tumor accumulation and retention level can be observed. It should be noted that only a small portion of NGs retained in
30 livers and were completely cleared in other main organs.

NIR light exhibits high tissue penetration enabling high absorption by ICG molecules in tumor tissue.^{24,25,51} Thus, photothermal-induced temperature increase and stimuli-triggered drug release can be achieved. To further elucidate the synergistic effect of photothermal-chemotherapy and NIR light-triggered drug release, we further investigated *in vivo* therapeutic efficacy of DINGs using subcutaneously transplanted H22 tumor model. The NGs loading ICG and/or DOX were injected intravenously into the mice at the dose of 200 μL containing comparable amount of ICG or DOX followed by NIR irradiation for 5 min at 24 h post-injection. After total three injections (day 0, 2, and 4) and three NIR irradiations (day 1, 3, and 5), the antitumor results were measured. As shown in Fig. 6A, the control group of PBS and free DOX did not show statically significant differences in tumor growth suppression. The groups treated using INGs with NIR irradiation or DINGs without NIR irradiation displayed slow tumor growth within 8 days and then the tumors grew quickly, indicating that these formulations showed moderate therapeutic efficacy and cancer cells were not killed efficiently. In contrast, the group treated by DINGs with NIR irradiation showed complete tumor growth suppression. The
45 tumor sizes were shrunk to be significantly smaller within 16 days revealing superior therapeutic efficacy (Fig. 6B). Histological analysis of tumor tissues by H&E staining exhibited significantly looser tissue structures after treatment by DINGs under NIR irradiation as compared with other treatment groups (DINGs and INGs + NIR) which applied single chemotherapy or photothermal therapy, respectively (Fig. S4). The superior therapeutic efficacy of DINGs under NIR irradiation should be attributed to synergistic effect of photothermal-chemotherapy and
50

NIR light-triggered drug release.

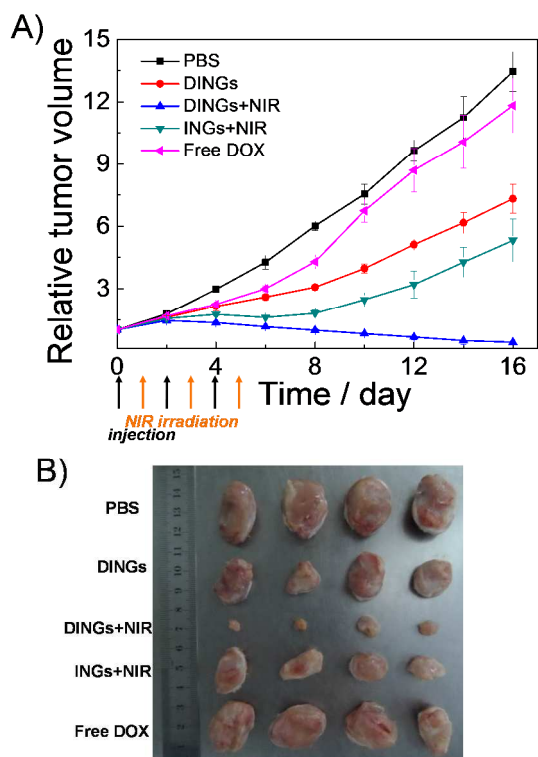


Fig. 6 *In vivo* antitumor efficacy of various treatment groups. (a) Relative tumor volume of H22-bearing mice after treatments with varying formulations. Three injections on days 0, 2 and 4 were conducted, and NIR irradiation for 5 min was performed at 24 h post-injection. Data are expressed as mean \pm SD, $n = 4$. (b) Photographs of the tumors collected from varying groups of mice at the end of treatments (day 16).

Conclusions

In summary, NIR light-triggered drug release systems were developed based on host-guest associated NGs. With simultaneous encapsulation of ICG and DOX, the EEs and LEs of ICG and DOX were both increased dramatically. DINGs showed pronounced photothermal effect under 805 nm NIR laser irradiation, resulting in temperature increase as well as NGs relaxation and dissociation. Thus, NIR light-triggered drug release can be achieved. Synergistic effect of photothermal-chemotherapy based on NIR light-triggered drug release NGs system showed superior tumor growth suppression. Moreover, in view of deep tissue penetration as compared with UV or visible light, this NIR-triggered drug release NG system showed great potentials for *in vivo* combined photothermal-chemotherapy applications.

Acknowledgements

The financial support from National Natural Scientific Foundation of China (NNSFC) Project (51273188, 81201176), A Foundation for the Author of National Excellent Doctoral Dissertation of PR China (FANEDD) (201224), the Specialized Research Fund for the Doctoral Program of Higher Education (SRFDP) (20123402120022), the Fundamental Research Funds for the Central Universities (WK2060200012) is gratefully acknowledged.

Notes and references

- ^a Key Laboratory of Functional Molecular Solids, Ministry of Education, 35 Anhui Key Laboratory of Molecule-based Materials, College of Chemistry and Materials Science, Anhui Normal University, Wuhu, Anhui, China. E-mail: shzhuo@mail.ahnu.edu.cn.
- ^b CAS Key Laboratory of Soft Matter Chemistry, Department of Polymer Science and Engineering, University of Science and Technology of China, 40 Hefei, Anhui 230026, China. Tel: +86-551 63603670; E-mail: gezs@ustc.edu.cn.
- ^c Department of Ophthalmology, Hospital of Anhui Province, Hefei, Anhui 230001, China. Email: luodanld@hotmail.com.
- † Electronic Supplementary Information (ESI) available: Fig. S1-S4. See 45 DOI: 10.1039/b000000x/
- 1 D. Peer, J. M. Karp, S. Hong, O. C. Farokhzad, R. Margalit and R. Langer, *Nat. Nanotechnol.*, 2007, **2**, 751.
 - 2 M. E. Davis, Z. Chen and D. M. Shin, *Nat. Rev. Drug Discovery*, 2008, **7**, 771.
 - 3 N. Kamaly, Z. Y. Xiao, P. M. Valencia, A. F. Radovic-Moreno and O. C. Farokhzad, *Chem. Soc. Rev.*, 2012, **41**, 2971.
 - 4 H. Cabral and K. Kataoka, *J. Controlled Release*, 2014, **190**, 465.
 - 5 S. Mura, J. Nicolas and P. Couvreur, *Nat. Mater.*, 2013, **12**, 991.
 - 6 Z. S. Ge and S. Y. Liu, *Chem. Soc. Rev.*, 2013, **42**, 7289.
 - 7 A. K. Bajpai, S. K. Shukla, S. Bhanu and S. Kankane, *Prog. Polym. Sci.*, 2008, **33**, 1088.
 - 8 C. D. H. Alarcon, S. Pennadam and C. Alexander, *Chem. Soc. Rev.*, 2005, **34**, 276.
 - 9 N. Fomina, J. Sankaranarayanan and A. Almutairi, *Adv. Drug Delivery Rev.*, 2012, **64**, 1005.
 - 10 J. F. Gohy and Y. Zhao, *Chem. Soc. Rev.*, 2013, **42**, 7117.
 - 11 B. Yan, J. C. Boyer, N. R. Branda and Y. Zhao, *J. Am. Chem. Soc.*, 2011, **133**, 19714.
 - 12 K. Konig, T. W. Becker, P. Fischer, I. Riemann and K. J. Halhuber, *Opt. Lett.*, 1999, **24**, 113.
 - 13 J. Cao, S. Huang, Y. Chen, S. Li, X. Li, D. Deng, Z. Qian, L. Tang and Y. Gu, *Biomaterials*, 2013, **34**, 6272.
 - 14 J. Liu, C. Detrembleur, B. Grignard, M. C. De Pauw-Gillet, S. Mornet, M. Treguer-Delapierre, Y. Petit, C. Jerome and E. Duguet, *Chemistry-an Asian Journal*, 2014, **9**, 275.
 - 15 J. You, R. P. Shao, X. Wei, S. Gupta and C. Li, *Small*, 2010, **6**, 1022.
 - 16 M. S. Yavuz, Y. Cheng, J. Chen, C. M. Copley, Q. Zhang, M. Rycenga, J. Xie, C. Kim, K. H. Song, A. G. Schwartz, L. V. Wang and Y. Xia, *Nat. Mater.*, 2009, **8**, 935.
 - 17 R. Chen, X. C. Zheng, H. Q. Qian, X. Wang, J. Wang and X. Q. Jiang, *Biomater. Sci.*, 2013, **1**, 285.
 - 18 H. Y. Chen, X. M. Chi, B. W. Li, M. Zhang, Y. X. Ma, S. Achilefu and Y. Q. Gu, *Biomater. Sci.*, 2014, **2**, 996.
 - 19 J. H. Park, G. von Maltzahn, L. L. Ong, A. Centrone, T. A. Hatton, E. Ruoslahti, S. N. Bhatia and M. J. Sailor, *Adv. Mater.*, 2010, **22**, 880.
 - 20 M. L. Viger, W. Sheng, K. Dore, A. H. Alhasan, C. J. Carling, J. Lux, C. de Gracia Lux, M. Grossman, R. Malinow and A. Almutairi, *Acc Nano*, 2014, **8**, 4815.
 - 21 M. P. Melancon, M. Zhou and C. Li, *Acc. Chem. Res.*, 2011, **44**, 947.
 - 22 L. Wu, S. T. Fang, S. Shi, J. Z. Deng, B. Liu and L. T. Cai, *Biomacromolecules*, 2013, **14**, 3027.
 - 23 H. Yang, H. J. Mao, Z. H. Wan, A. J. Zhu, M. Guo, Y. L. Li, X. M. Li, J. L. Wan, X. L. Yang, X. T. Shuai and H. B. Chen, *Biomaterials*, 2013, **34**, 9124.
 - 24 M. B. Zheng, C. X. Yue, Y. F. Ma, P. Gong, P. F. Zhao, C. F. Zheng, Z. H. Sheng, P. F. Zhang, Z. H. Wang and L. T. Cai, *Acc Nano*, 2013, **7**, 2056.
 - 25 Z. H. Wan, H. J. Mao, M. Guo, Y. L. Li, A. J. Zhu, H. Yang, H. He, J. K. Shen, L. J. Zhou, Z. Jiang, C. C. Ge, X. Y. Chen, X. L. Yang, G. Liu and H. B. Chen, *Theranostics*, 2014, **4**, 399.
 - 26 Q. Chen, C. Liang, C. Wang and Z. Liu, *Adv. Mater.*, 2015, **27**, 903.
 - 27 M. Guo, H. J. Mao, Y. L. Li, A. J. Zhu, H. He, H. Yang, Y. Y. Wang, X. Tian, C. C. Ge, Q. L. Peng, X. Y. Wang, X. L. Yang, X. Y. Chen, G. Liu and H. B. Chen, *Biomaterials*, 2014, **35**, 4656.
 - 28 K. Miki, T. Inoue, Y. Kobayashi, K. Nakano, H. Matsuoka, F. Yamauchi, T. Yano and K. Ohe, *Biomacromolecules*, 2015, **16**, 219.
 - 29 J. X. Zhang and P. X. Ma, *Adv. Drug Delivery Rev.*, 2013, **65**, 1215.

- 30 L. F. Fraceto, R. Grillo and E. Sobarzo-Sanchez, *Curr. Top. Med. Chem.*, 2014, **14**, 518.
- 31 M. M. Zhang, X. Z. Yan, F. H. Huang, Z. B. Niu and H. W. Gibson, *Acc. Chem. Res.*, 2014, **47**, 1995.
- 5 32 M. Xue, Y. Yang, X. D. Chi, Z. B. Zhang and F. H. Huang, *Acc. Chem. Res.*, 2012, **45**, 1294.
- 33 A. Hashidzume and A. Harada, *Polym. Chem.*, 2011, **2**, 2146.
- 34 G. Chen and M. Jiang, *Chem. Soc. Rev.*, 2011, **40**, 2254.
- 35 J. H. Lee, K. J. Chen, S. H. Noh, M. A. Garcia, H. Wang, W. Y. Lin,
10 H. Jeong, B. J. Kong, D. B. Stout, J. Cheon and H. R. Tseng, *Angew. Chem., Int. Ed.*, 2013, **52**, 4384.
- 36 H. Wang, S. T. Wang, H. Su, K. J. Chen, A. L. Armijo, W. Y. Lin, Y. J. Wang, J. Sun, K. Kamei, J. Czernin, C. G. Radu and H. R. Tseng, *Angew. Chem., Int. Ed.*, 2009, **48**, 4344.
- 15 37 M. Fang, J. H. Zhang, Q. L. Wu, T. W. Xu and Y. Y. Cheng, *J. Phys. Chem. B*, 2012, **116**, 3075.
- 38 S. T. Wang, K. J. Chen, T. H. Wu, H. Wang, W. Y. Lin, M. Ohashi, P. Y. Chiou and H. R. Tseng, *Angew. Chem., Int. Ed.*, 2010, **49**, 3777.
- 20 39 M. V. Rekharsky and Y. Inoue, *Chem. Rev.*, 1998, **98**, 1875.
- 40 M. Shokeen, E. D. Pressly, A. Hagooley, A. Zheleznyak, N. Ramos, A. L. Fiamengo, M. J. Welch, C. J. Hawker and C. J. Anderson, *Acs Nano*, 2011, **5**, 738.
- 41 J. Strohalm and J. Kopecek, *Angew. Makromol. Chem.*, 1978, **70**,
25 109.
- 42 M. Semsarilar, V. Ladmiral, A. Blanazs and S. P. Armes, *Langmuir*, 2012, **28**, 914.
- 43 I. Lengyel, V. Cesare and T. Taldone, *Synth. Commun.*, 2001, **31**, 2499.
- 30 44 G. Tripodo, C. Wischke, A. T. Neffe and A. Lendlein, *Carbohydr. Res.*, 2013, **381**, 59.
- 45 H. Arima, F. Kihara, F. Hirayama and K. Uekama, *Bioconjugate Chem.*, 2001, **12**, 476.
- 46 C. Kojima, Y. Toi, A. Harada and K. Kono, *Bioconjugate Chem.*,
35 2008, **19**, 2280.
- 47 M. Guo, J. Huang, Y. B. Deng, H. Shen, Y. F. Ma, M. X. Zhang, A. J. Zhu, Y. L. Li, H. Hui, Y. Y. Wang, X. L. Yang, Z. J. Zhang and H. B. Chen, *Adv. Funct. Mater.*, 2015, **25**, 59.
- 48 X. H. Zheng, F. F. Zhou, B. Y. Wu, W. R. Chen and D. Xing, *Mol. Pharm.*, 2012, **9**, 514.
- 40 49 E. Engel, R. Schraml, T. Maisch, K. Kobuch, B. Koenig, R. M. Szeimies, J. Hillenkamp, W. Baumler and R. Vasold, *Invest. Ophthalm. Vis. Sci.*, 2008, **49**, 1777.
- 50 M. Urbanova, A. Sturcova, J. Kredatusova and J. Brus, *Int. J. Pharm.*, 2014, **478**, 464.
- 45 51 R. Weissleder, *Nat. Biotechnol.*, 2001, **19**, 316.